

# Computing Strains Due to Screening Currents in REBCO Magnets

Dylan J Kolb-Bond, Edgar Berrospe-Juarez , Mark Bird , Senior Member, IEEE, Iain R. Dixon , Senior Member, IEEE, Hubertus W. Weijers , Senior Member, IEEE, Frederic Trillaud, Victor M. R. Zermeno, and Francesco Grilli 

**Abstract**—Screening currents have long been known to impact the stress state in tape-wound superconducting coils. In recent years the advent of REBCO tape has led to the development of tape-wound coils by a number of organizations. While several groups have been computing screening currents and ac losses in REBCO tape in a variety of applications for several years, little has been published about the stress due to the screening currents. This problem is challenging due to the need to analyze thousands of REBCO turns which are not bonded together. The T-A formulation of Maxwell’s equations employing a homogenization technique enables efficient estimation of the current distribution while structural calculations employing contact elements allow conservative estimation of stresses. Computational results are compared with observed degradation in a test coil. Future coil designs that include the effects of screening current strains are proposed

**Index Terms**—Coupled mechanical and electromagnetic analysis, 2G HTS magnet, large-scale superconductor systems.

## I. INTRODUCTION

THE strains resulting from screening currents are extremely important to understand with regards to high field magnet design using REBCO tapes due to the large computed strains and observed plasticity in test coils. Screening currents in HTS tapes occur because changing magnetic fields generate electric currents with critical values to oppose the changing field. These currents form a loop where on one side of the tape it adds to the

Manuscript received September 22, 2019; accepted February 13, 2020. Date of publication March 10, 2020; date of current version April 22, 2020. This work was supported in part by the National High Magnetic Field Laboratory, in part by NSF cooperative agreement DMR-1644779, in part by the State of Florida in part by the Programa de Maestría y Doctorado en Ingeniería de the Universidad Nacional Autónoma de México (UNAM), in part by the Consejo Nacional de Ciencia y Tecnología (CONACYT) under CVU: 490544, and in part by the Dirección General de Asuntos del Personal Académico (DGAPA) - UNAM through PAPIIT-2017 (#TA100617) and PAPIIT-2019 (#IN107119). (Corresponding author: Mark Bird.)

Dylan J Kolb-Bond, Mark Bird, Iain R. Dixon, and Hubertus W. Weijers are with the National High Magnetic Laboratory, Tallahassee, FL 32310 USA, and also with the Florida State University, Tallahassee, FL 32306 USA (e-mail: kolb-bond@magnet.fsu.edu; bird@magnet.fsu.edu).

Edgar Berrospe-Juarez and Frederic Trillaud are with the Universidad Nacional Autónoma de México, CDMX, Mexico city 04510, Mexico.

Victor M. R. Zermeno is with the NKT GmbH & Company KG 51061, Cologne, Germany.

Francesco Grilli is with the Karlsruhe Institute of Technology 76131 Karlsruhe, Germany.

Color versions of one or more of the figures in this article are available online at <http://ieeexplore.ieee.org>.

Digital Object Identifier 10.1109/TASC.2020.2979396

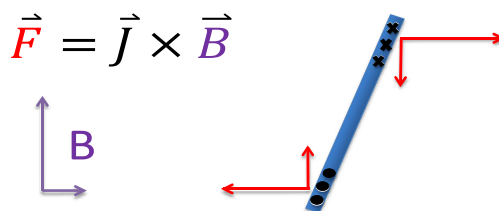


Fig. 1. Screening current vectors and resultant Lorentz forces at the top and bottom of the tape.

transport current and on the other side subtracts from it. Fig. 1 shows schematically the cross section of a tape with screening current,  $J$ , concentrated on the edges flowing in and out of the page, a large vertical and small horizontal magnetic field,  $B$ , and the resultant Lorentz forces,  $F$ . The Lorentz force on these screening current loops creates a torque that can lead to large hoop strains that are possibly detrimental to the magnet’s life.

Screening currents are known to affect the performance of the systems, reducing the central field by means of the so-called “screening current induced field” (SCIF) noted in [1] affecting homogeneity and central field magnitude and producing hysteresis losses [2], [3]. The effect of screening currents on the stresses and strains are a recent addition to the analysis. Previous inquiries into screening current induced stresses and strains include [4], [5] who showed that the hoop strain might be 2-3x greater when including the effects of screening currents, well beyond the 0.6–0.7% strain levels typically associated with both critical current degradation and plasticity. This type of damage to the REBCO tape was observed in some disks of the prototype coil “20/70” at the NHMFL. The “20/70” prototype coil was a test coil that achieved 22.5 T in a 15 T background field [12]. When unwound, damage to the tape was observed in “waviness” and  $I_c$  degradation indicating the coil was operated in a high strain state. The analysis results shown in Section IV. suggest that the damage could be the result of screening strains during normal operation. These results alone show that screening strains are vitally important to both understand and control in order to build high field magnets and will need to be included in all analysis of future high field REBCO coils.

The analysis herein uses the T-A homogenized method [3] to efficiently compute the electromagnetic data before mapping the Lorentz forces onto a structural submodel that includes

TABLE I  
STRESS ANALYSIS MODEL KEY PARAMETERS

Material Parameters	Thickness, width [mm]	$(E_r, E_z, E_\theta)$ [GPa]
REBCO tape	0.165, 4	67, 97, 97
Cowind	0.025, 4	200, 200, 200
Mandrel	1.5, 4	15, 15, 15
Overband	1, 4	200, 200, 200

"20/70" Parameters	Values	Units
Inner radius, outer radius	20, 70	mm
Number of disks	12	
Turns per disk	244	
Operating current	200	A
Background field	15	T

refined geometry and boundary conditions. Improvements from prior analysis [4], [5] are made with the use of tuned contact elements between each turn and more realistic modeling of the geometry and boundary conditions. Suggestions are made to aid in designing future coils with the effects of screening currents by utilizing critical current ( $I_c$ ) grading.

## II. ANALYSIS METHOD

The goal of this analysis is to compute the strains resulting from screening currents, with specific attention to the "20/70" coil, with key parameters shown in Table I. This requires the coupling of an electromagnetic and structural model. The electromagnetic model was created in COMSOL Multiphysics because of its connection with MATLAB and the ability to solve coupled PDE's. The structural model was created in ANSYS because the ANSYS Parametric Design Language (APDL) language is capable of modelling the complex geometry required and has historically been used in structural analysis. Because of the complicated nature of the screening torque it is not currently practical, in a stress analysis, to accurately model an entire coil at a time. The process then is to compute the electromagnetic data for a whole coil system and then apply the resulting Lorentz forces to a structural model of each disk separately.

Electromagnetic data ( $J$ ,  $B_r$ ,  $B_z$ ) is computed in COMSOL Multiphysics using the T-A homogenous method and output for each turn of each disk with 121 divisions along the 4 mm width. Fig. 2 shows the computed current density data  $J$  for disk #4 of the "20/70" coil. This data is imported into EXCEL and transformed into a matrix for each data component ( $J$ ,  $B_r$ ,  $B_z$ ) at each node for each individual disk using a Visual Basic macro. Using EXCEL to interface between the two Finite Element Analysis (FEA) models allows these data matrices to be plotted, post-processed, and output into a usable form for the stress analysis in ANSYS simultaneously. The data is then imported into ANSYS and homogenized from the 1D, 1  $\mu\text{m}$  REBCO layer to a conductor width and thickness, then averaged in each axial element division for each conductor turn. The averaged current density for a single tape at the ID using an axial element

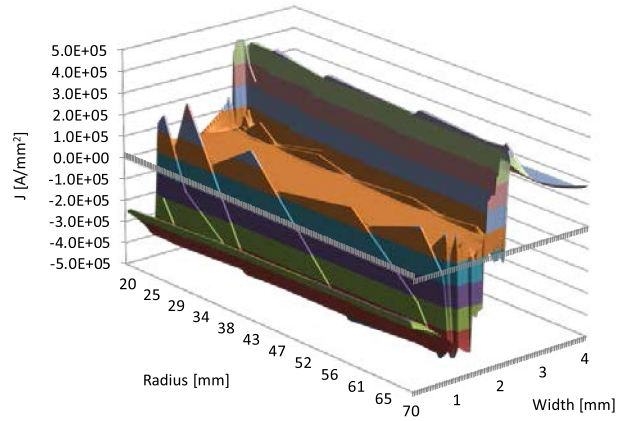


Fig. 2. Surface plot of the current density in disk #4 of "20/70" coil. Color bands aid in distinguishing amplitude.

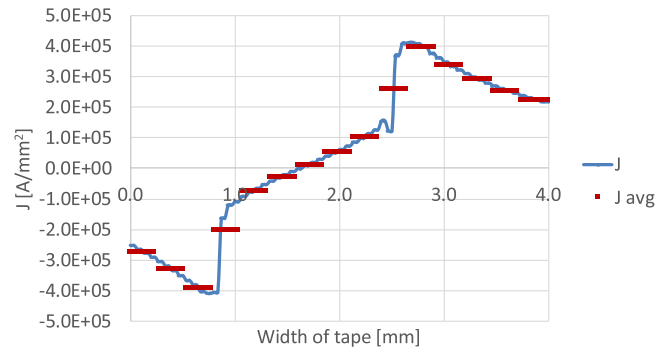


Fig. 3. Averaged current density and original current density data for a single tape at the ID.

count of 15 is shown in Fig. 3. The Lorentz force density is calculated and applied in the stress analysis model as the radial and axial components of  $\vec{J} \times \vec{B}$ . This sub modeling allows the electromagnetic model to be simplified immensely by the T-A homogeneous model while being able to refine the structural model, ultimately reducing the overall computation time.

## III. STRESS ANALYSIS MODEL

The FEA structural model needs to accommodate the complicated nature of screening torques. Because of the torque on each individual conductor turn, tapes must be allowed to slide and separate. This requires modeling of each conductor and co-wind turn to avoid unrealistic shear stress and tensions between adjacent turns. For one example calculation, bonding conductor to co-wind reduced the peak strain from 0.98% to 0.95% while bonding two conductor and co-wind pairs together reduced the strain from 0.98 to 0.77%. The fully bonded case only resulted in 0.44% strain. In all but the most extreme cases of radial compression the use of contact elements is required to account for turn-to-turn separation. These contact elements allow neighboring turns to separate or transmit forces if contact occurs. During contact, the contact elements act as nonlinear

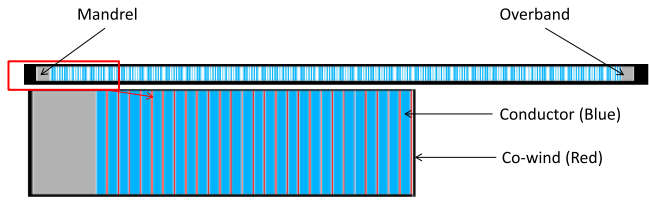


Fig. 4. Geometry of a structural model, shows conductor, co-wind, mandrel, and overband for a single pancake wound disk.

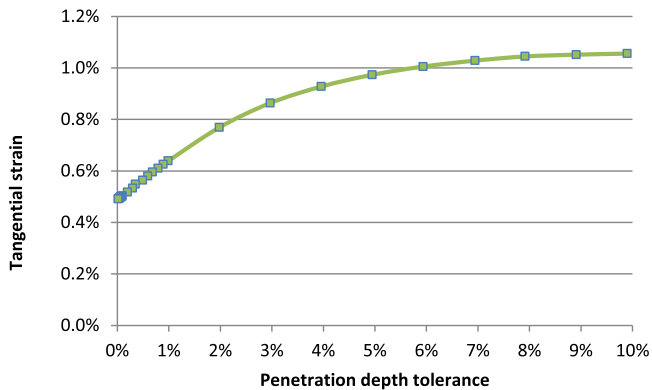


Fig. 5. Strain vs. Penetration depth tolerance for an example coil with moderate radial compression.

springs with a large stiffness calculated as a function of the elastic modulus and penetration depth.

Using ANSYS, the geometry is modeled for each conductor and co-wind turn, the winding mandrel and overbanding as shown in Fig. 4. The geometry is meshed with many axial divisions ( $>15$ ) to allow the current density direction change to be represented accurately with the average shown in Fig. 3 and allow accurate calculation of bending strains while avoiding prohibitive computation times. Contact elements are applied on each axial element division between each conductor and co-wind turn, and between the mandrel and overbanding. The contact elements used represent surface-to-surface contact and are symmetric to allow penetration between conductor to co-wind and co-wind to conductor. Contact elements should be tuned by minimizing the penetration depth tolerance to allow convergence but also accurate results. Because of the thickness of the REBCO tapes used ( $\sim 100 \mu\text{m}$ ) it is important to set the penetration depth tolerance (FTOLN in APDL) to a small fraction of the tape thickness ( $<1\%$ ) especially when there is radial compression in the windings. Assuming the default FTOLN is used (10% of thickness) the difference in calculated hoop strain can be as large as  $2x$  as shown in Fig. 5. where only the FTOLN parameter is modified. Because the contact algorithm maintains that the final penetration depth is less than the allowable tolerance [11] every tape can penetrate up to the tolerance in the radial direction which leads to a summation of radial displacements for every turn and unnaturally large hoop strains.

Material properties of a linear elastic modulus and Poisson's ratio are set for an orthotropic conductor, isotropic mandrel,

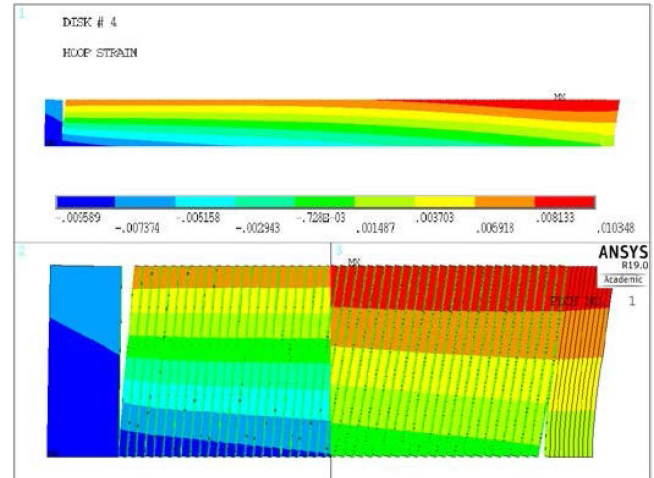


Fig. 6. ANSYS results for disk #4 of the 20/70 coil. Damage is predicted to occur in the orange and red regions. Color gauge shows strain from  $-0.96\%$  to  $+1.0\%$ . White space shows separation between components.

co-wind, and reinforcement. The boundary conditions applied are an axial displacement of 0 at the radially outer, bottom edge of each conductor and co-wind tape to allow the other bottom edge to move in the axial direction due to the vertical Lorentz force component. It is not unreasonable to treat each conductor and co-wind pair as bonded together and give an axial displacement constraint of 0 to the entire bottom edge (“roller” condition) [3] as that is computationally faster and easier to converge but less accurate in most cases where radial tension exists inside the radial build of the coil and the vertical Lorentz force is greater than the axial compression. Applying this “roller” condition to the entire bottom edge artificially reduced the strain from  $0.82\%$  to  $0.65\%$  in one calculation. The constraints on the mandrel and overband are an axial displacement of 0 at the bottom edge (“roller”).

The electromagnetic data ( $J$ ,  $B_r$ ,  $B_z$ ) is imported disk by disk into ANSYS. Conductor by conductor, the currents and fields are averaged in each element division according to their height and radius. The average current density is homogenized from the  $1 \mu\text{m} \times 4 \text{ mm}$  REBCO layer to the conductor width and thickness as the ratio of the thicknesses  $J_h = J_r * t_c/t_r$ . Where  $J_h$  and  $t_c$  are the homogenized current density and conductor thickness,  $J_r$  and  $t_r$  are the current density in REBCO layer and REBCO layer thickness ( $1 \mu\text{m}$ ). The Lorentz force density is then calculated as  $\vec{J} \times \vec{B}$  and applied to that element division. This method of sub modeling generalizes the structural model to accommodate any discretization of electromagnetic input data for that coil. The model is then solved.

#### IV. RESULTS

Computed strains for “20/70” coil using this approach show peak strains above  $1.0\%$  and large sections of the tape width above yield strength. Fig. 6 shows hoop strain calculations for disk #4, which predicts plastic deformation at the OD of the

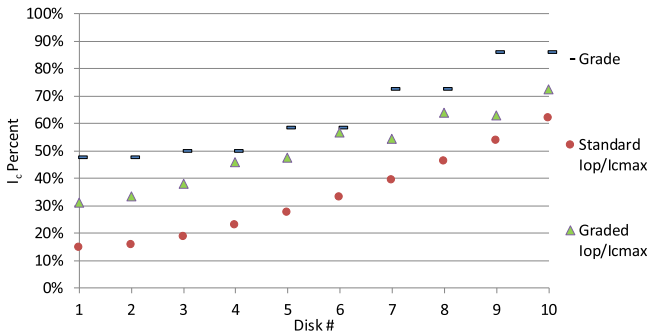


Fig. 7. Critical current scaling and computed fraction of critical current in a test coil, for standard and graded tapes with disks numbered from midplane to end.

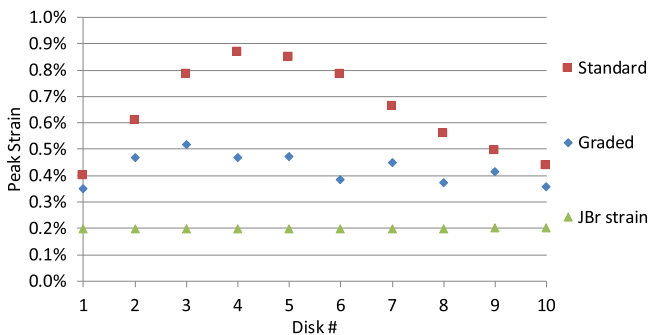


Fig. 8. Computed peak strains in a test coil design with standard and graded  $I_c$  tapes compared with strain considering only transport current.

disk. Comparing these calculations with experimental data is difficult with the lack of strain measurements but the calculations seem to correlate well with degradation observed in the “20/70” coil, which was plastically deformed at the OD of disk # 4, where the highest region of yield strain was computed. Other test coils have been unwound after testing and have observed plastic deformation of the tape. [7].

Including the screening strain in future designs has begun with an 11.75 T HTS insert test coil design that is planned to be operated in a 14 T background coil to achieve 25.75 T. By using critical current grading of individual disks, the goal is to operate the coil at a high fraction of critical current ( $I_{op}/I_{cmax}$ ) to reduce the screening currents and resultant strains. Fig. 7 shows the “grade” of conductor specified for each disk as well as the resulting maximum fraction of  $I_c$  that will occur in each disk for standard and graded tapes. The grading of the tape assumes tape can be purchased with an arbitrary reduction of  $I_c$  given  $J_c = \beta * J_{c0}$  [3] where  $\beta$  is an arbitrary constant.

Plotting the peak strains in the test coil design while changing only the critical current grading between standard  $I_c$  and graded  $I_c$  shows a 45% reduction in peak strain alone. Fig. 8 Compares three computed strain values: 1) the simple  $JBr$  value which ignores screening currents and underestimates the strain, 2) the strain in a coil with standard  $I_c$  including screening currents as described herein, and 3) a coil with  $I_c$  grading and including the effects of screening currents. Looking at the distribution

of peak strains across the axial length of the coil without  $I_c$  grading shows that the maximum strain of a coil occurs not at the midplane, where the maximum  $JBr$  strain occurs, nor at the end of the coil where the radial field is maximum, but midway up the coil, noted in [5], where the  $I_c$  and driving radial field  $B_r$  intersect.

## V. DISCUSSION

It is unknown how much the peak strain area affects the overall performance of the tape. The peak strain value can be high but also occupy a small fraction of the tape width while the rest of the tape width is much lower strain and can reverse into compression. It is suggested that the large regions at yield strain are the culprit for the observed plastic deformation which agrees with the waviness observed in the “20/70” coil.

However,  $I_c$  degrades before plastic deformation [8]. As a result, actual screening currents would be less than computed here, reducing the torque and strain. This could lead to the conductor self-stabilizing. The degradation and plastic deformation is omitted in the model which uses a linear elastic modulus for the conductor and does not consider  $I_c$  degradation as a function of hoop strain which would require the structural model to be dynamically coupled to the electromagnetic model.

The results here omit many important factors that have the capability to be included in a stress analysis that would be beneficial to the strain distribution. These effects include winding tension, thermal contraction, bending strain, axial compression; friction between turns and turn spacers, and the tape tilting redistributing screening currents. These effects should overall improve the strain by pre-compression, decreasing sliding between turns and limiting screening currents. As a result these results are overly conservative but still seem fairly consistent with experimental results and also useful for design of future magnets. Other technologies worth investigating would be multi-filamentary REBCO tapes [6] and grading the co-wind of individual disks based on the peak strain plot above as in Fig. 8. Screening strains are now being included in future magnet designs by grading the critical currents to specific values and adding more reinforcement to reduce the strain from transport current while allowing a greater margin for screening current effects.

## VI. CONCLUSION

A method has been developed to compute screening currents in COMSOL Multiphysics and map them into ANSYS to compute the strains associated with them. This method of sub modeling allows practical computation times while maintaining the complexity of both models. The computed strains predict deformation in test coils and seem to correlate with observed degradation. A promising technology to reduce the strain from screening effects is critical current grading. Due to the possibility of high strain, it is necessary to include screening strains in the design of all future high field REBCO coils.

## REFERENCES

- [1] Y. Yanagisawa *et al.*, "Effect of YBCO-coil shape on the screening current-induced magnetic field intensity," *IEEE Trans. Appl. Supercond.*, vol. 20, no. 3, pp. 744–747, Jun. 2010.
- [2] F. Grilli, E. Pardo, A. Stenvall, D. Nguyen, W. Yuan, and F. Gömöry, "Computation of losses in HTS under the action of varying magnetic fields and currents," *IEEE Trans. Appl. Supercond.*, vol. 24, no. 1, Feb. 2014, Art. no. 8200433.
- [3] E. B.-Juarez, V. M. R. Zermeno, F. Trillaud, and F. Grilli, "Real-time simulation of large-scale HTS system: Multi-scale and homogeneous models using the *T-A* formulation," *Supercond. Sci. Technol.*, vol. 32, no. 6, Art. no. 065003, <https://doi.org/10.1088/1361-6668/ab0d66>
- [4] J. Xia, H. Bai, H. Yong, H. W. Weijers, T. A. Painter, and M. D. Bird, "Stress and strain analysis of a REBCO high field coil based on the distribution of shielding current," *Supercond. Sci. Technol.*, vol. 32, Jul. 2019, Art. no. 095005.
- [5] Y. Li *et al.*, "Magnetization and screening current in an 800-MHz (18.8-T) REBCO NMR insert magnet: Experimental results and numerical analysis," *Supercond. Sci. Technol.*, <https://doi.org/10.1088/1361-6668/ab3119>
- [6] Y. Yanagisawa, Y. Xu, X. Jin, H. Nakagome, and H. Maeda, "Reduction of Screening current-induced magnetic field of REBCO coils by the use of multi-filamentary tapes," *IEEE Trans. Appl. Supercond.*, vol. 25, no. 3, Jun. 2015, Art. no. 6603705.
- [7] S. Hahn *et al.*, "45.5-tesla direct-current magnetic field generated with a high temperature superconducting magnet," *Nature*, vol. 570, pp. 496–499, 2019.
- [8] Y. Zhang *et al.*, "Stress–Strain relationship, critical strain (stress) and irreversible strain (stress) of IBAD-MOCVD-based 2G HTS wires under uniaxial tension," *IEEE Trans. Appl. Supercond.*, vol. 26, no. 4, Jun. 2016, Art. no. 8400406.
- [9] W. Markiewicz *et al.*, "Design of a superconducting 32 T magnet with REBCO high field coils," *IEEE Trans. Appl. Supercond.*, vol. 22, no. 3, Jun. 2012, Art. no. 4300704.
- [10] E. Berrospe-Juarez *et al.*, "Screening currents and hysteresis losses in the REBCO insert of the 32 T All-superconducting magnet using T-A homogenous model," presented at the Int. Conf. Magn. Technol. (MT26), Vancouver, Canada, 2019.
- [11] ANSYS, "ANSYS contact technology guide", Nov. 2004.
- [12] M. Breschi, L. Cavalucci, P.L. Ribani, A. V. Gavrilin, and H. W. Weijers, "Analysis of quench in the NHMFL REBCO prototype coils for the 32T magnet project," *Supercond. Sci. Technol.*, vol. 29, Mar. 2016, Art. no. 055002.